Elsevier Editorial System(tm) for NeuroImage
Manuscript Draft

Manuscript Number: NIMG-13-2074R1

Title: The dynamics of contour integration: A simultaneous EEG-fMRI study

Article Type: Regular Article

Section/Category: Cognitive Neuroscience

Corresponding Author: Mr. Bogdan Mijovic,

Corresponding Author's Institution: Katholieke Universiteit Leuven

First Author: Bogdan Mijovic

Order of Authors: Bogdan Mijovic; Maarten De Vos, Professor; Katrien Vanderperren, PhD; Bart Machilsen, PhD; Stefan Sunaert, Professor; Sabine Van Huffel, Professor; Johan Wagemans, Professor

Abstract: To study the dynamics of contour integration in the human brain, we simultaneously acquired EEG and fMRI data while participants were engaged in a passive viewing task. The stimuli were Gabor arrays with some Gabor elements positioned on the contour of an embedded shape, in three conditions: with local and global structure (perfect contour alignment), with global structure only (orthogonal orientations interrupting the alignment), or without contour. By applying JointICA to the EEG and fMRI responses of the subjects, new insights could be obtained that cannot be derived from unimodal recordings. In particular, only in the global structure condition, an ERP peak around 300 ms was identified that involved a loop from LOC to the early visual areas. This component can be interpreted as being related to the verification of the consistency of the different local elements with the globally defined shape, which is necessary when perfect local-to-global alignment is absent. By modifying JointICA, a quantitative comparison of brain regions and the time-course of their interplay was obtained between different conditions. More generally, we provide additional support for the presence of feedback loops from higher areas to lower level sensory regions.

1. Cover Letter

INGENIEURSWETENSCHAPPEN
ELEKTROTECHNIEK (ESAT-SCD(SISTA))
KASTEELPARK ARENBERG 10 – BUS 2446
B-3001 LEUVEN

KU LEUVEN

To the Editor of NeuroImage

OUR REF. Oct 01, 2013
YOUR REF.
LEUVEN

Dear Editor,

Please find enclosed the revised version of our paper, “The dynamics of contour integration: A simultaneous EEG-fMRI study”, Bogdan Mijović, Maarten De Vos, Katrien Vanderperren, Bart Machilsen, Stefan Sunaert, Sabine Van Huffel and Johan Wagemans.(NIMG-13-2074).

With this letter, we would like to express our thanks to the reviewers and yourself for the helpful and positive comments on our manuscript. We have carefully considered each of the comments and responded to these in the attached answer to the reviewers. In addition, all fragments in the manuscript that have been modified accordingly, have been indicated in red.

We hope that we have satisfactorily addressed the questions and points raised by the reviewers and truly hope for a positive evaluation.

Sincerely Yours,

Bogdan Mijović

BOGDAN MIJOVIĆ
TEL. + 32 16 32 17 99 FAX + 32 16 32 19 70
bogdan.mijovic@esat.kuleuven.be
www.esat.kuleuven.be/scd/biomed

ASSOCIATIE K.U.LEUVEN

*3. Reviewer Suggestions

Suggested Reviewers

Zoe Kourtzi,
Cognitive Neuroimaging Lab
University of Birmingham
Email: Z.Kourtzi@Bham.ac.uk

Mafred Fahle,
Zentrum für Kognitionswissenschaften
Universität Bremen
Email: mfahle@uni-bremen.de

Michael Herzog,
Laboratory of Psychophysics
EPFL
Email: michael.herzog@epfl.ch

Ilona Kovacs,
Budapest University of Technology and Economics
Department of Cognitive
Email: ikovacs@cogsci.bme.hu

Highlights

* New insights in perceptual grouping with simultaneous EEG-fMRI
* A modified group ICA method for analyzing different conditions together is presented.
* Analysis identified presence of activity around 300 ms when viewing global contours without local alignments.
* Further evidence for feedback activity from higher cortical areas to lower sensory regions.

We would like to thank the academic editor for the time and effort spent on reading our paper and handling its review process. We would also like to thank the reviewers for their insightful and helpful comments. We took into account their concerns and suggestions in the revised manuscript. We hope we managed to address all the suggestions in an appropriate way. Please find our detailed explanation below in response to the specific points.

Reviewers' comments:

Reviewer #1: I thank the authors for addressing my previous comments. However, I believe there remain some amenable issues. In the following I refer to my previous major comments (1) - (3) and minor comment (1). In summary, I think that the documentation and explanation of the methods and results can still be improved.

Major comments

(1) With respect to the interpretation of the JointICA findings in light of "recurrent interactions" and "predictive coding", the authors acknowledge that "this interpretation is largely speculative at this point". In my view, it would therefore be appropriate not to highlight "reverse hierarchies" and "predictive coding" in the manuscript's abstract.

- ***Reply:*** **Thank you for this remark. We removed the disputed highlights from the manuscript's abstract.**

(2) If I interpret the JointICA percent signal change (PSC) maps correctly, these are derived from the concatenated data over participants, which were subjected to IC decomposition and data set reconstruction based on selected components [I may be in error here, because this issue is not documented very well. In fact, there are some occasions at which the authors refer to significance testing over subjects. If the latter is the case, the results can of course readily be statistically evaluated based on group statistics. Adding to my confusion is the fact that there is indeed a reference to p-values in Figure 7]. The null distribution, which the authors base their interpretation of "significant signal change" on, is then derived from the distribution of reconstructed PSC values over voxels. I would assume that some of the voxels exceeding "3 times the standard deviation of the map" do this to a higher degree (e.g. 4 times) than others (e.g. 3.5 times). To allow for a numeric evaluation of the study's results (e.g. with respect to possible meta-analyses), I believe it would be helpful to derive some kind of suitable summary measure that allows for the evaluation of the relative strength of the topographic activations and document this in tabular form alongside the MNI coordinates.

- ***Reply:*** **Thank you for this remark. Indeed, the numerical values can help the evaluation of the results. The numbers are added now in a tabular form (Table 2), alongside with the MNI coordinates.**

(3) The authors cite the study by Schwarzkopf et al. J Neurophys (2009) on p.25 with respect to fMRI-adaptation. However, the respective study was not based on an fMRI-adaptation paradigm, but used a multi-voxel pattern analysis approach and GLM-based activation methods. Because of the high similarity of the stimuli and conditions employed, I believe a more in-depth treatment of converging and contrasting findings between the authors' study and the work by Schwarzkopf et al. would be appropriate.

- ***Reply:*** **Thank you for this remark. Indeed, the study is an example of an MVPA fMRI study, not an fMRI-adaptation study. We apologize for the mistake. The reviewer notes a high similarity of the stimuli and conditions employed but, in fact, there are major differences too. The paths in Schwarzkopf et al. (2009) are five parallel straight and open contours, whereas we use one single curved and closed contour. For the alignment of Gabor elements on the path, there are similarities between the two studies. The "collinear" condition in Schwarzkopf et al. is similar to our LG condition, and their "orthogonal" condition is comparable to our GO condition (although we alternate between orthogonal and collinear elements). The most relevant data in Schwarzkopf et al. are the pre-training data (reported only in Supplemental Material) for the collinear and orthogonal conditions. We now discuss these in somewhat more detail in the present revision. Note, however, that we cannot do this in greater detail because some of the results are not reported at the group level (only showing individual results in their Figure S9).**

Minor comments

(1) I thank the authors for addressing this point and now have a clearer understanding of the analyses performed. However, in line with my major comment (2) above, the documentation of the 2nd level GLM analyses could be improved by providing a summary in tabular-numeric, rather than only pictorial, form. Additionally, because the PSC measures derived from the GLM parameter estimates form the basis of the JointICA results, I think the paper could benefit from explicitly stating the

PSC formula and possibly relating this to the concept of percent global signal change as discussed in Gläscher J "Visualization of Group Inference Data in Functional Neuroimaging" Neuroinform (2009) 7: 73-82, p. 78.

- ***Reply:*** **We added another table to show the GLM results in a tabular form (Table 1). In this table, we also provide the T-scores of the strongest activated voxel.**

  Comparing our calculations to the paper the reviewer has mentioned, the way we compute the PSC is not the percent global signal change, but rather a percent local signal change as the author of that paper suggests.

  i.e.: "rfxplot alleviates these two problems and computes PSC by taking the mean signal intensity of the tissue type into account which is captured in the voxel-specific and session-wide constant term in a first level analysis. rfxplot computes PSC with the following equation:

  PSC =(Bmax * max(HRF) * 100) / Bconst

  where β task is the parameter estimate of the condition of interest in the voxels of interest, max(HRF) is the maximum of a regressor with a single event, and β const is the parameter estimate of the session-wide constant for the particular voxels of interest. In that sense, the PSC computed by rfxplot can be regarded as a measure of Percent Local Signal Change which expresses how much a particular voxel is activated by an experimental conditions compared to its own baseline."

  To avoid any misunderstandings, here we provide the exact way we computed the PSC:

  1) If X is the design matrix and C is the contrast vector depicting the contrast of interest,
  then D is the event of interest regressor, a matrix depicting a subpart of the design matrix, with number of rows equal to the number of scans and the number of columns equal to the regressors involved in the contrast (if multiple runs, each relevant condition for each run will be included; if more then one basis function per single condition or trial type are

included in the contrast, all will be included in D)

2) The event regressor D is in principle multiplied by the estimated voxel weights (voxels by regressors), yielding the signal change in time associated with this event.

This mulitplication is done for each regressor in D separately, and because we want the amplitude of the response associated with trials of a particular type, we take the peak amplitude of the regressor (ie when the response is highest) and multiply it by the beta associated with that regressor, yielding one response strength value (instead of a time series of values) for a particular regressor.

3) The response amplitude for a regressor expressed as a percentage of the mean signal intensity in the voxel, ie., the value stored in the betas maps that correspond to the session specific constants in the last column(s) of the design matrix X. This gives a percentage signal change for that regressor (in that voxel)

4) This procedure is repeated for each regressor in the contrast, and the average response strength value is computed as THE response strength associated with the event or contrast. (In contrasts with opposite conditions (e.g., 0 0 1 0 0 -1, ...), the mean give the difference between the conditions involved)

In formula form:

PSCi = Σd=1:r [(Betadi * max(Dd)) / Gbetadi] / d
with D = X*C
d = index of regressors (columns in D)
Gbetadi = the global signal for voxel i in session that regressor Dd belongs to.

We also added the formula to the text.

Reviewer #2: It would be helpful to include the vector lengths and normalization details in the manuscript (e.g. the info provided in response to the question "What were the lengths of the ERP and fMRI vectors that went into the joint ICA? Were the vectors normalized"). I am confused by the response to :"Page 19, last two sentences: There does not appear to be a 70 ms response in the NC condition". The authors seem to acknowledge that this is true but the manuscript still

states that this response exists (e.g. "After condition-specific back-reconstruction, this source shows in all three conditions a similar positive deflection around 70 ms in the ERP ... similar sources are active in the different conditions".

- ***Reply:*** **We are sorry that we overlooked this. It is corrected now in the text. As for the vector lengths, they are also added to the manuscript.**

*7. Manuscript
Click here to view linked References

The dynamics of contour integration: A simultaneous EEG-fMRI study

Authors: Bogdan Mijović[a,b,*], Maarten De Vos[a,d], Katrien Vanderperren[a,b], Bart Machilsen[c], Stefan Sunaert[e], Sabine Van Huffel[a,b], Johan Wagemans[c]

[a] KU Leuven, Department of Electrical Engineering, STADIUS, Leuven, Belgium.

[b] KU Leuven, iMinds Future Health Department, Leuven, Belgium.

[c] KU Leuven, Laboratory of Experimental Psychology, Leuven, Belgium.

[d] Oldenburg University, Department of Psychology, Neuropsychology Lab, Oldenburg, Germany.

[e] KU Leuven, Department of Radiology, Leuven, Belgium.

[*] Corresponding author: Bogdan Mijović

Kasteelpark Arenberg 10 - box 2446, B-3001 Leuven, Belgium.

Tel: +3216321799. Fax: +3216321970.

E-mail address: bogdan.mijovic@esat.kuleuven.be

Keywords: Contour Integration, Shape Detection, Vision, EEG-fMRI Integration, Data Driven Methods

Abstract

To study the dynamics of contour integration in the human brain, we simultaneously acquired EEG and fMRI data while participants were engaged in a passive viewing task. The stimuli were Gabor arrays with some Gabor elements positioned on the contour of an embedded shape, in three conditions: with local and global structure (perfect contour alignment), with global structure only (orthogonal orientations interrupting the alignment), or without contour. By applying JointICA to the EEG and fMRI responses of the subjects, new insights could be obtained that cannot be derived from unimodal recordings. In particular, only in the global structure condition, an ERP peak around 300 ms was identified that involved a loop from LOC to the early visual areas. This component can be interpreted as being related to the verification of the consistency of the different local elements with the globally defined shape, which is necessary when perfect local-to-global alignment is absent. By modifying JointICA, a quantitative comparison of brain regions and the time-course of their interplay was obtained between different conditions. More generally, we provide additional support for the presence of feedback loops from higher areas to lower level sensory regions.

Introduction

To successfully interact with the environment our brain transforms the pattern of light on the retina into meaningful and coherent representations of the objects, scenes and events in the world. To decide which parts of the visual input belong together, and which parts belong to separate objects or to the background, our visual system relies on grouping principles such as proximity, similarity, and collinearity. These grouping principles have been introduced by the Gestalt psychologists early last century (for review, see Wagemans et al., 2012), and reflect the statistical properties of our natural environment (Elder & Goldberg, 2002; Geisler, 2008).

In the present study we investigate the neural mechanisms underlying the grouping principle of collinearity or "good continuation" (Wertheimer, 1923) in shape perception: the tendency to link spatially aligned neighboring elements into a continuous string. This process, referred to as contour integration, is crucial to detect borders between distinct image regions. An effective method for studying contour integration is the pathfinder or snake detection paradigm (Field, Hayes, & Hess, 1993), which requires participants to detect a smooth contour in a background of randomly positioned Gabor elements. Psychophysical studies have demonstrated that contour integration depends on the separation and orientation of the local elements relative to the global path trajectory (Hess & Field, 1999).

Some authors have argued that a reinforcing cascade of lateral connections between orientation tuned cells in the primary visual cortex (V1) provides the neural substrate for contour integration (e.g., Li & Gilbert, 2002). However, a serial propagation through intrinsic horizontal connections in V1 might be too slow to account for fast modulatory influences by stimuli far outside the classical receptive field of V1 cells (Angelucci & Bressloff, 2006). Most likely, contour integration is mediated partly by extrastriate feedback connections to V1 (Angelucci et al., 2002). This feedback from higher

visual areas could also explain the sensitivity of V1 neurons to the shape of spatially extended contours (McManus, Li, & Gilbert, 2011), especially when the contours form closed shapes.

The contribution of both striate and extrastriate areas to contour integration has also been observed in functional magnetic resonance imaging (fMRI) studies. Gabor elements that are arranged in closed shapes elicit stronger BOLD responses than randomly oriented Gabor elements, in the object-sensitive lateral occipital complex (LOC) as well as in early visual areas (Altmann et al., 2003; Kourtzi et al., 2003), suggesting a feedback mechanism from higher to lower visual areas. Although fMRI can inform us about which cortical areas are involved in contour integration, it does not allow tapping into the temporal aspects of the grouping processes, and the dynamic interplay between feedforward and feedback processes. Electro-encephalography (EEG) and magneto-encephalography (MEG), on the other hand, have good temporal resolution but insufficient spatial precision.

The goal of the current study was to identify fine spatiotemporal interactions between the different cortical regions involved in contour integration and shape detection, and to provide further evidence for feedback from LOC to early visual regions, by exploiting simultaneous EEG-fMRI measurements. A critical aspect of this study, compared to previous work, is that we have combined contour integration with shape detection, and that we have compared conditions in which local element linking is part of contour integration with conditions in which the contour of a global shape emerges only at a higher level.

Materials and Methods

Participants

Fifteen participants (eight male, seven female; mean age 27.4 years) with no history of neurological or cardiological disorders volunteered for this study. All participants reported normal or corrected-to-normal vision and gave written informed consent. The study was approved by the KU Leuven Ethics Committee.

Stimuli and conditions

We used MATLAB (v 7.1; The MathWorks, Natick, MA, USA) and GERT, the Grouping Elements Rendering Toolbox (Demeyer & Machilsen, 2012), to construct arrays of non-overlapping Gabor elements on a uniform grey background (Figure 1). The arrays comprised 496 × 496 pixels. During the experiment the arrays were presented centrally and subtended approximately 10° of visual angle. Each Gabor element was defined as the product of a sine wave luminance grating (frequency of 3 cycles per degree of visual angle) and a circular Gaussian (standard deviation of 3 arc min). A subset of 45 Gabor elements was positioned along the contour outline of an artificial shape. The shape outlines were generated by plotting the sum of 5 radial frequency components in polar coordinates, with each component having a random phase angle and amplitude. After rescaling the surface area to one eighth of the array size we co-localized the center of mass of each shape with the center of the array. This procedure yielded shapes of intermediate complexity, not too homogenously convex but also not with too many salient protrusions or indentations.

Next, the remainder of the array was populated with Gabor elements. The number of elements inside and outside the shape outline was adjusted for each shape to ensure a homogeneous spacing between the Gabor elements. The number of interior elements ranged between 60 and 72, the number of exterior elements between 507 and 542. No stimuli were included for which the mean local density – here defined as the average Euclidean distance from each element to its five nearest neighbors – differed more than 1 arc min between interior, contour, and exterior elements. This

procedure yielded displays with uniform element density, which necessitates grouping based on element orientation.

In each array all interior and exterior elements had the same orientation. Three different stimulus types were obtained by manipulating the orientations of elements on the contour (Figure 1). In the *local and global* (***LG***) condition (panel A), all contour elements were aligned along the outline of the embedded shape. In other words, each pair of adjacent contour elements is *locally* aligned, and the entire set of contour elements results in a perceptually closed *global* shape. In that condition, local edge linking at a lower level could give rise at an integrated shape percept at a higher level. In the *global only (**GO**)* condition (panel B), only half of the contour elements were aligned along the outline of the embedded shape and every other element was oriented perpendicular to the shape outline. This still yields a global percept of a closed contour, albeit somewhat weaker, but without the local alignment between adjacent contour elements. In other words, in this condition, local edge linking is made impossible and the global shape can only emerge at a higher level, either by linking only every other element (requiring orientation coupling across larger distances) or by treating the local elements only as place markers while ignoring the orientation of half of the elements. In the *no contour (**NC**)* condition (panel C), all elements on the embedded shape outline were oriented parallel to the other elements in the array, giving rise to a uniform texture with no visible contour or shape.

Figure 1. Example stimuli used in the experiment. (A) *local and global* stimulus, obtained by orienting the elements on the contour parallel to the local tangent at the contour. (B) *global only* stimulus, in which every other contour element alternates between an orientation parallel to or orthogonal to the shape outline. (C) *no contour* stimulus, in which all Gabor elements have the same orientation. (D) *catch* stimulus, which is always a no-contour stimulus with a small circle overlaid at a random location. Catch trials are not included in the analyses.

Task and procedure

Participants engaged in a passive viewing task. They fixated in the middle of the screen while the stimuli were displayed on a uniform gray background. To ensure that participants attended the displays we introduced an undemanding orthogonal catch task. Participants were instructed to press a response button when a circle was present in the array (Figure 1D). The location of the circle varied across catch trials. Catch trials were not included in the analyses.

An experimental run lasted about 5 minutes, and consisted of contour trials (frequency = .24), no contour trials (frequency = .48), catch trials (frequency = .08), and blank trials (dummy trials) in which no stimuli were presented at all (frequency = .20). There were exactly 120 structure trials, 240 non-structure trials, 40 catch trials and 100 blank trials per condition (LG | GO). LG and GO conditions were presented in separate runs, 4 of each type. The stimulus order within each run was optimized using the approach suggested by Kao et al. (2009). A GO or LG contour stimulus was always preceded by 1 to 5 NC stimuli with identical Gabor positions, and was always followed by a NC stimulus with different Gabor positions. All the NC stimuli had different orientations of Gabor elements and we therefore do not expect any low-level adaptation to the NC stimuli. To make sure that any effect pertains only to differences in element orientation (and not to differences in element position), the first NC stimulus following a GO or LG contour stimulus was not included in our analyses. The positions of Gabor elements in successive NC arrays did not change, but their orientations did (each element was rotated at least 30 degrees away from its previous orientation).

Each stimulus was presented for 200 ms. The duration of the inter-trial interval was uniformly sampled between 2000 and 2400 ms. A central fixation cross was shown during the inter-trial interval. The experiment was run with the Presentation software (Neurobehavioral Systems, Albany,

CA, USA). A Barco 6400i LCD projector was used to present the stimuli on a translucent screen attached to the bore of the scanner. Participants saw the stimuli via a mirror attached to the head-coil.

Functional MRI

fMRI acquisition

To acquire the functional MRI (fMRI) data we used a Philips 3-T Intera scanner (Royal Philips Electronics, Amsterdam, the Netherlands) with an eight-channel SENSE head-coil. For each experimental run 155 echo-planar images (EPI) were recorded with 2 s repetition time (TR) and 30 ms echo time (TE). To ensure whole-brain coverage each EPI contained 36 slices of 3 × 3 × 3 mm voxel size. In addition to the EPIs, a full brain anatomical image was obtained with the magnetization-prepared rapid acquisition with gradient echo (MP-RAGE) imaging sequence (182 coronal slices, TR = 9.7 s, TE = 4.6 ms, 1 × 1 × 1 mm voxel size).

fMRI preprocessing

fMRI analyses were performed with the statistical parametric mapping software (SPM8, Wellcome Trust Centre for Neuroimaging, London, UK). The EPIs were slice-time corrected, realigned, co-registered with the MP-RAGE, and then normalized to MNI space using the ICBM152 T1-weighted template, and smoothed with a 6-mm FWHM Gaussian kernel. Next, fMRI activation maps were obtained via a general linear model (GLM) analysis with stick-functions based on the onset times of the different stimuli. The stick functions were used to model each condition separately. The stick functions are then convolved with the canonical HRF (double gamma) as implemented in SPM8

package to obtain the final regressors. More specifically, the percent signal change (PSC) data were computed voxel-wise from the betas estimated in the single subject single task GLM analysis as a voxel's condition specific beta weight relative to its session specific beta weight. The PSC computation is done according to Equation (1) in the same way as the percent local signal change was computed in Gläscher, 2009. The unthresholded PSC maps were the input for the subsequent JointICA analysis.

$$PSC = (\beta_{max} \cdot max(HRF) \cdot 100)/\beta_{const} \quad (1)$$

Localizer runs

In addition to the 8 experimental runs focusing on contour integration, we ran 4 localizer runs, designed to accurately define a number of retinotopic and shape-selective brain areas that we assume to be involved in the visual processing of our contour integration stimuli. The acquisition parameters differed slightly from the experimental runs. For the localizer runs we recorded 110 EPIs with 48 slices at a TR of 3 s and a TE of 30 ms.

Two runs were used to localize early visual areas V1 and V2 with a standard meridian mapping technique. Horizontal and vertical wedges composed of checkerboard and circular patterns were presented to the participants. The patterns alternated at 2.66 Hz. These stimuli specifically activate the borders between early retinotopic areas. In the remaining two localizer runs we presented intact and scrambled versions of familiar objects. Each stimulus was presented for 750 ms. The contrast between intact and scrambled images can be used to extract the lateral occipital complex, an occipitotemporal region involved in the representation of a perceived object shape (e.g., Grill-Spector et al., 1998).

Definition of regions of interest

To define the regions of interest (ROIs), the anatomical images of all participants were first segmented and flattened using the caret5 software (Van Essen Laboratory, Washington University, St. Louis, USA). Subsequently, SPM contrast maps from the object-localizer and meridian-mapping runs were projected on these flat maps, and thresholded based on a *p*-value of 0.001. The resulting overlays allowed defining the LOC (including the lateral occipital cortex, LO, and the posterior fusiform gyrus, pFs) for the object-localizer runs, and areas V1 and V2 for the meridian-mapping runs. Group ROIs were defined as the region where the individual ROIs from at least 10 participants spatially overlapped.

Electrophysiology

EEG acquisition

The EEG data were collected in the scanner from 62 standard scalp sites using the MR-compatible BrainAmp MR+ system (BrainProducts, Munich, Germany), at a sampling rate of 5 kHz. Two additional electrodes were placed below the left eye and on the left upper back to monitor eye blinks and the electrocardiogram, respectively. All 64 channels were recorded with FCz as reference and Iz as ground. Electrode impedances were kept below 10 kΩ. The clock of the MR system was down-sampled to pace the clock of the EEG acquisition computer using commercially available hardware (SyncBox, Brain Products). The start of each volume was automatically marked in the EEG data.

EEG preprocessing

Preprocessing of the raw EEG data was done in the EEGLAB software (v. 5.03; Delorme & Makeig, 2004). First, scanner-related gradient artifacts were reduced with the average template subtraction method (Allen et al., 2000), as implemented in the Bergen EEG-fMRI EEGLAB plug-in (Moosmann et al., 2009). After filtering the data between 1 and 30 Hz and downsampling to 250 Hz, scanner-related ballistocardiogram artifacts were reduced with a combination of the Optimal Basis Set method (Niazy et al., 2005) and ICA (Vanderperren et al., 2010). In addition, eye movement artifacts were reduced with ICA (Joyce et al., 2004; De Vos et al., 2011), all the removed components were manually checked, and data were re-referenced to the average of TP9 and TP10 (the electrodes closest to the mastoids in our electrode setup).

To extract event-related potentials (ERPs), all available blocks per participant and per condition were merged together and data were segmented from 100 ms before until 500 ms after stimulus onset. Baseline correction was performed based on the 100 ms pre-stimulus interval and low quality trials were rejected by thresholding trials at 150 μV. Finally, an average ERP for each stimulus type was computed.

Using the above-mentioned methods, the scanner-related artifacts in the ERP are significantly reduced. We provide the plots of the average ERP's together with the standard deviations in the top panel of Fig. 2. From this figure, it is apparent that a sufficient artifact reduction from the ERP data has been achieved to allow for further processing.

Data analysis Part I - Joint ICA for each stimulus category

To extract spatio-temporal information from the simultaneously acquired EEG and fMRI data different data integration approaches can be applied. For a consistent overview, we refer the reader to Huster et al., (2012). In this work we make use of JointICA, a principled and data-driven approach

to multimodal data integration. The technique was originally introduced by Calhoun et al. (2006), and has recently been validated by Mijović et al. (2012). JointICA starts from the assumption that encephalographic and hemodynamic responses co-vary.

To apply the JointICA we first vectorized the fMRI PSC map for every participant and stimulus condition and concatenated this with the average ERP at a specific channel for the same participant and stimulus condition. The vectors were approximately 150,000 samples long (the ERP data were upsampled to fit the length of the fMRI data). The data were Z-transformed. The ERP and fMRI data were normalized separately. We always used electrode Oz as the channel of interest, as this occipital electrode appears to be well-suited for the analysis of visual processes with JointICA (Mijović et al., 2012). This electrode was chosen for 2 main reasons: 1) It is centrally suited, so it measures the activity in both left and right cortex equally, and 2) From (Mijović et al., 2012), where PO7 and PO8 electrodes were also explored, Oz was the only electrode to be able to unravel the activity in EVA, which is crucial in this study. We then built for each condition a matrix with the subject-specific concatenated fMRI-EEG vectors as rows. This matrix was demixed using the JointICA algorithm (freely available from http://icatb.sourceforge.net), resulting in joint independent component maps as in Equation (2). These joint independent component maps incorporate both spatial and temporal information about the neural sources involved in processing of our stimuli.

$$[X^{fMRI}\ X^{EEG}] = A \cdot [s^{fMRI}\ s^{EEG}] \qquad (2)$$

After estimating the mixing matrix A, the sources can be extracted by

$$s = A^{-1} \cdot X\ . \qquad (3)$$

Next, the sources of interest are selected based on their energy contribution, such that the selected sources together explain more than 85% of the total energy in both ERP and fMRI modalities. Finally, the back-reconstruction of a particular source was achieved by simply setting all other sources to zero, and computing X_{br} as

$$X_{br} = A \cdot s_i\ . \qquad (4)$$

The reliability of the JointICA decomposition was checked by calculating the stability index (*Iq*) using ICASSO (Himberg et al., 2004), as proposed by Mijović et al. (2012). The *Iq* index was computed for all independent components, both based on the complete dataset (15 participants), and when one of the participants was left out. In addition, this ICASSO analysis allowed us to estimate the number of underlying components, based on the computation of the R-index (Himberg et al., 2004). A reliability index higher than 0.9 implies a robust decomposition (Mijović et al., 2012).

Data analysis Part II - Simultaneous JointICA for all stimulus categories together

In the above analysis we performed the traditional JointICA on the data of each condition separately. However, our three stimulus conditions and the processes induced by them show certain similarities, and hence it can be expected that they share some underlying neural sources. A separate demixing for each stimulus condition makes it difficult to identify the common sources, and at the same time complicates the extraction of unique, condition-specific sources. It would therefore be advantageous to estimate the mixing matrices and sources for all three conditions simultaneously. As such, this modified JointICA can reveal the similarities and peculiarities between conditions.

To explain our approach in more detail, let us denote the matrices representing the EEG and fMRI data from all participants, induced by condition LG, with X_{LG}^{EEG} and X_{LG}^{fMRI}, respectively (and analogously for the conditions GO and NC). We then combine the data from the different conditions in a single matrix and perform the ICA analysis, as shown in Equation (5):

$$\begin{bmatrix} X_{LG}^{fMRI} & X_{LG}^{EEG} \\ X_{GO}^{fMRI} & X_{GO}^{EEG} \\ X_{NC}^{fMRI} & X_{NC}^{EEG} \end{bmatrix} = \begin{bmatrix} A_{LG} \\ A_{GO} \\ A_{NC} \end{bmatrix} \cdot \begin{bmatrix} s^{fMRI} & s^{EEG} \end{bmatrix} , \qquad (5)$$

with A_{LG}, A_{GO} and A_{NC} the parts of the mixing matrix *A* corresponding to the conditions LG, GO and

NC, respectively, and s^{EEG} and s^{fMRI} the EEG and fMRI portions of the extracted independent components. For similar processes across conditions, the A_{LG}, A_{GO} and A_{NC} parts of the mixing matrix will be similar for the three conditions. For a process unique to a specific condition, the mixing coefficients of this particular condition will differ from the other two conditions. This modification of the JointICA algorithm assesses the information embedded in the source signals jointly for all conditions.

We can then use the condition-specific parts of the estimated mixing matrix to back-reconstruct the sources for a particular condition. For example, by multiplying the inverse of the LG-specific part of the mixing matrix *A* with the EEG and fMRI data from this same condition, the independent sources for the LG condition can be extracted. This is illustrated in Equation (6), where A_{LG}^{-1} is the pseudo-inverse of the LG-specific part of the mixing matrix.

$$\left[s_{LG}^{fMRI}\ s_{LG}^{EEG}\right] = A_{LG}^{-1} \cdot \left[X_{LG}^{fMRI}\ X_{LG}^{EEG}\right] \quad (6)$$

As before, we use the energy criterion to disregard noise components. Next, we can detect which sources are common to two or three conditions and which ones are unique to a single condition by comparing the distribution coefficients of a particular independent component across subjects. If the component's distribution coefficients are significantly higher in one condition compared to the other conditions, we conclude that this particular component is unique to this condition. If the component shows a similar distribution across subjects for two or more conditions, we conclude that this process is common for these conditions. Statistical significance is formally tested using paired *t*-tests.

Results

We first present the results of a traditional, single-modality analysis of our EEG and fMRI data, as if the data for each modality were acquired in a separate session. Next, we describe the results of a multimodal analysis of EEG and fMRI data using JointICA. Finally, we apply our modification of the JointICA approach to estimate the weighting matrices for all three stimulus conditions simultaneously. In the discussion of our results, we emphasize the comparison between the two contour conditions (GO and LG), which is of most importance to this particular study.

Unimodal EEG and fMRI data analyses

In this section, we describe the results of a unimodal analysis of (simultaneously recorded) EEG or fMRI data, thereby ignoring the other modality. Figure 2 graphically presents the condition-specific ERP and fMRI signals, averaged across subjects. The top panel of Figure 2 shows the grand average ERPs on channel Oz for each stimulus condition. The shaded area represents the standard deviation across subjects. The scalp distributions of these grand average ERPs are displayed in the middle panel, at a latency of 90 ms (top) and 190 ms (bottom) after stimulus onset. The bottom panel shows fMRI results of a second-level SPM analysis on a lateral and medial view of an inflated template brain. The colored lines in these same figures represent the borders of the group ROIs V1, V2 and LOC. For this and all subsequent figures we only show the right hemisphere, because we could not reliably define the left hemisphere's ROIs in all participants. The T-scores, alongside with the MNI values of the strongest activated voxel in a particular area in the bottom panel of Figure 2, are given in Table 1.

Figure 2. Top panel: Condition-specific grand average (N=15) ERPs (LG = local and global; GO = global only; NC = no contour) on channel Oz. The shaded area represents the standard deviation across subjects. The vertical axes in both ERP and scalp maps are given in microvolts. Middle panel: Scalp distributions at the 2 time points indicated by the vertical lines in the top panel: around 90 ms (blue, top) and around 190 ms (red, bottom) after stimulus onset. Bottom panel: Results from a 2nd-level SPM analysis on the fMRI data, showing the effect of each condition relative to fixation (p=0.01, uncorrected), together with the group ROIs V1, V2 and LOC. The color bar describes the T-values of the functional maps. These group ROIs are defined as the region of overlap between individual ROIs from at least 10 out of 15 participants.

Table 1. The T-scores, alongside with the MNI coordinates of the strongest activated voxel for the 2nd level SPM analysis from the bottom panel of Figure 2.

The grand mean ERPs in the top panel of Figure 2 display a distinct pattern that is similar across conditions. The shape of these waveforms is typical for visual evoked potentials, with a first positive deflection at about 100 ms (P1), followed by a negativity between 150 and 200 ms (N1). The topography in the middle panel reveals that these deflections are mainly located over occipital electrode sites. These observations are in line with the results of a previous study where we measured the EEG response to similar Gabor displays outside the scanner (Machilsen et al., 2011). The fMRI maps in the bottom panel show activity in occipital and occipitotemporal regions. All three stimulus conditions activate areas V1 and V2, as well as the lateral occipital complex. Several fMRI studies have previously reported that both retinotopic and occipitotemporal areas are involved in contour integration (e.g., Altmann et al., 2003; Kourtzi et al., 2003). The results of our unimodal fMRI analysis are consistent with the univariate analyses reported by Schwarzkopf et al. (2009). Their contrast between collinear stimuli (comparable to our LG condition) and jittered stimuli (comparable

to our NC condition) only revealed differences in higher visual areas (including object-sensitive regions), not in early visual areas.

By looking at the pair-wise contrasts shown in Figure 3, we find that both LG and GO differ only in LOC compared to NC (Kourtzi et al., 2003). No clear difference in fMRI activity is observed between the LG and GO conditions. From this unimodal analysis we could conclude that both stimulus types are processed in a similar fashion. However, the LG and GO conditions do have a different ERP waveform, with the largest difference at about 200 ms. The difference in ERP suggests that the processing of LG and GO stimuli is not identical, but that different processes (maybe even in different brain areas) are involved at different time points. The difference in fMRI suggests that the difference between LG and NC is larger than the difference between GO and NC, especially in the more anterior parts of LOC. The goal of the multimodal analysis is to unravel this spatiotemporal pattern further.

Figure 3. Group-level differences between our three experimental conditions. From left to right: LG - GO, LG - NC, GO - NC. Top panel: ERP difference waves for electrode Oz. The shaded area represents 1.96 standard errors. Bottom panel: differences between fMRI PSC maps (p=0.01, uncorrected) plotted on an inflated MNI template. The borders of our group ROIs V1, V2 and LOC are drawn as solid lines.

Multimodal analysis using JointICA

The JointICA results are shown in Figures 4-6 for the conditions LG, GO and NC, respectively. As explained above, for each case, the stability index Iq from the ICASSO analysis was computed for the complete dataset as well as after leaving out one participant. In all cases, the calculated values were

higher than 0.9, implying a good reliability of the obtained results. The R-index of the ICASSO analysis estimated that we need to derive 15 components in order to have a stable decomposition, for all three conditions in this study. This does not imply, however, that all the 15 components were meaningful. the time-points shown in the figures and discussed below are solely determined by the JointICA method.

Figure 4 shows both the temporal (ERP) and spatial (fMRI) part of five back-reconstructed independent components resulting from applying JointICA to the data from the LG condition. Together with the ERP part of the independent components, also the grand average ERP corresponding to this same condition is shown. The components are ordered according to their temporal behavior.

From this figure, it becomes clear that in the LG condition both V1 and V2 (together referred to as the early visual areas or EVA) are activated around 70 ms and 200 ms (panels 1 and 4, respectively). The LOC area is mainly activated around 200 ms (panel 4) but also around 70 ms and 170 ms (panels 1 and 3). In addition, negative visual activations are visible around 130 ms and 170 ms (panels 2 and 3). These negatively activated areas indicate that the ERP and fMRI components are "anti-correlated", meaning that larger ERP peaks correspond to smaller fMRI activations and vice-versa.

Figure 4. Results of the JointICA analysis applied to the data in response to the LG stimulus. Five different components are shown, ordered according to their temporal contribution. For each component the upper panel of the figure shows the spatial (fMRI) part, whereas the bottom panel represents the temporal (ERP) part together with the average ERP waveform (solid versus dotted line, respectively). The fMRI figures show yellow-orange colors for positive activations and blue ones for deactivations and also

include the contours of the ROIs of interest in the same colors as in Figure 2. Only activations, of which the absolute value exceeds 3 times the standard deviation of the activation values in all voxels, are shown.

In a similar way as for the LG condition in Figure 4, Figure 5 shows the JointICA results from the data corresponding to the GO condition. For this condition, EVA activations are mainly found around 170 ms, 200 ms and 270 ms (panels 1, 2 and 3). Furthermore, the component found around 330 ms (panel 4) also shows additional EVA activation at this latency corresponding with a small peak at 70 ms. LOC activations are visible around 200 ms and 330 ms (panels 2 and 4). The activations around 170 ms and 200 ms are very similar to the activations shown earlier in Figure 4, but there is a clear difference visible in the ERPs around 330 ms. More specifically, at this latency there is a clear negative peak for the GO condition, which cannot be seen in the LG results. For the GO condition, this peak corresponds to activations in LOC and EVA.

Figure 5. Results of the JointICA analysis applied to the data in response to the GO stimulus. Four different components are shown, ordered according to their temporal contribution. For each component the upper panel of the figure shows the spatial (fMRI) part, whereas the bottom panel represents the temporal (ERP) part together with the average ERP waveform (solid versus dotted line, respectively). The fMRI figures show yellow-orange colors for positive activations and blue ones for deactivations and also include the contours of the ROIs of interest in the same colors as in Figure 2. Only activations, of which the absolute value exceeds 3 times the standard deviation of the activation values in all voxels, are shown.

The JointICA results for the NC condition are summarized in Figure 6. Also here, both the temporal

and spatial parts of the independent components are shown, the former together with the grand average ERP waveform. Here, EVA activations are found around 170 ms, 200 ms and 370 ms (panels 1, 2 and 3) and LOC activations around 170 ms and 200ms (panels 1 and 2). The late activation (around 370 ms) of the EVA ROI was also present for the LG condition (see Figure 4, panel 2), but in the case of the LG condition, the relation between ERP and fMRI activations was negative, whereas for the current condition (NC) it is positive.

Figure 6. Results of the JointICA analysis applied to the data in response to the NC stimulus. Three different components are shown, ordered according to their temporal contribution. For each component the upper panel of the figure shows the spatial (fMRI) part, whereas the bottom panel represents the temporal (ERP) part together with the average ERP waveform (solid versus dotted line, respectively). The fMRI figures show yellow-orange colors for positive activations and blue ones for deactivations and also include the contours of the ROIs of interest in the same colors as in Figure 2. Only activations, of which the absolute value exceeds 3 times the standard deviation of the activation values in all voxels, are shown.

Multimodal analysis using modified JointICA

To surpass qualitative, visual comparison between the JointICA results for the three stimulus conditions, Figure 7 illustrates the results of applying the modified JointICA approach to the data from all conditions simultaneously. The overview of the MNI coordinates of the peak activations for the corresponding maps is provided in Table 2. The number of independent sources to be derived was estimated to be 23. Six out of these 23 survived the energy-based selection criterion and are

shown in Figure 7. The upper part of the figure shows (from top to bottom) the condition-specific fMRI results for the LG, GO and NC condition, respectively. The condition-specific ERP results are shown below in the figure, together with their grand average ERP waveforms. Similar to Figures 4-6, back-reconstructed components are shown. However, in this case, back-reconstruction is done with only the condition-specific part of the mixing matrix. This allows the independent components, although estimated together, to differ between conditions. For example, the first column in Figure 7 shows the back-reconstruction of a source active around 70 ms. After condition-specific back-reconstruction, this source shows in both LG and GO conditions a similar positive deflection around 70 ms in the ERP, and significant activation in early visual areas in fMRI. However, we were unable to detect this component in NC condition. So at this point in time, similar sources are active in both contour conditions. The fifth column, describing the source active around 300 ms, shows clear differences after back-reconstruction. In the ERP, the back-reconstructed activity shows flat lines in LG and NC conditions, while a deflection is observed in the GO. This difference is due to the fact that the mixing vector for the LG and NC conditions contains very small values. The fMRI panels show active voxels for the GO condition, while no activations survived the threshold in the two other conditions. This implies that this source is unique to the GO condition. As explained before, a paired *t*-test is used to compare the condition-specific distributions across subjects for each component. The distributions, in this case, are the condition-specific columns of the mixing matrix, obtained by JointICA. In the figure, only *p*-values corresponding to significantly different distributions across subjects ($p < 0.05$) are included. Their subscripts specifically indicate the two conditions that were compared. In this way, we detect processes specific for only one or two conditions, as described in the Methods section.

The components in the first and third panel show the same distribution across subjects for the three conditions ($p > 0.05$). The component in the first panel shows activations in the early visual areas (EVA) around 70 ms after stimulus onset. This activation could not be separated in the original

JointICA analysis for the NC and GO conditions (Figures 5 and 6). The component in the third panel reveals activations in higher visual areas (LOC) around 200 ms. This same component was also found in the results obtained with the original JointICA analysis for all conditions (as shown in Figures 4-6).

The component in the second panel shows activations in the LOC and EVA ROIs around 170 ms after stimulus onset. Similar to the component shown in panel 3, also this component was found in the individual JointICA analyses for all conditions (see Figures 4-6). However, as opposed to this previously explained component, the distribution across subjects of the current one is significantly different for the LG and NC conditions, implying that the processes behind these activations are physiologically different. By closer look at the activated regions, it is obvious that, although the EVA and LOC ROIs are activated for all three conditions, the activation in the LOC is comparable for LG and GO, but different from NC. Also the activation of the EVA region is similar for LG and GO, but different for the NC condition. Although the difference between the ERP shapes is not apparent, their strengths are significantly different between the these condition.

The component presented in the fourth panel of Figure 7, with the ERP part peaking around 240 ms after stimulus onset, shows significantly different distributions across subjects for all three conditions. The NC-specific ERP part of this IC is a flat line with zero amplitude, implying no activation for this condition around this latency. The difference between the GO- and LG-specific parts of this IC is in the amplitude of their ERP peaks at 240 ms. In addition, the GO condition shows activations in the EVA areas, whereas for the LG condition, also the LOC area is activated.

The fifth panel of Figure 7 shows a component around 300 ms that is only characteristic for the GO condition, with activations in the LOC and EVA ROIs. This component corresponds to a component retrieved with the individual JointICA analysis for this condition, as can be seen from panel 4 in Figure 5. The advantage of the modified JointICA analysis, however, is that the flat lines available from the

LG- and NC-specific parts of the ERP information, confirm the exclusiveness of this component for the GO condition.

Finally, the rightmost panel of Figure 7 shows an IC around 370 ms with not significantly different distributions across subjects for the three conditions. All three conditions reveal activations in the EVA areas. However, the EVA ROI activations for the NC and GO conditions are positive, whereas these same activations are negatively related to the ERP waveforms for the LG condition. This observation could not be made based on the results from the individual JointICA analyses and suggests the presence of very late activations of the early visual areas specifically for GO and NC.

Figure 7. Results of the modified JointICA analysis, performed jointly on the data from all three conditions (LG = local and global, GO = global only and NC = no contour). The upper panels show the spatial (fMRI) results from the condition-specific independent components, for (from top to bottom) the LG, GO and NC conditions. For each case, the results are only depicted from those angles that show the major part of the activation (as before, only those parts of the activation are shown that exceed 3 times the standard deviation of all activation values). P-values are only mentioned if they are below 0.05. The bottom panel presents the temporal (ERP) parts of the independent components, with different colors distinguishing between the different conditions. These colors correspond to those used in Figures 4-6. Together with the independent components (solid line), also the grand average ERPs for all conditions are plotted (dashed line). Like in Figures 4-6, also here the components are ordered according to their temporal peak behavior. The empty fMRI sections in panels 4 and 5 correspond to components for which the ERP part is a flat line.

Table 2. The overview of the signal strength expressed in the multiples of standard deviation of the signal, alongside with the MNI coordinates of the peak activation corresponding to the maps shown in Figure 7. The MNI coordinates are provided for each ROI per component per condition.

Discussion

In the present study we investigated the temporal interactions between brain regions involved in contour integration and shape detection. Because a unimodal analysis of EEG and fMRI data is not able to unravel the full dynamics of the processes involved, we present an integrated analysis of EEG and fMRI data that can reveal the spatiotemporal differences between different perceptual processes induced by different stimulus conditions. Integration of EEG and fMRI data can be achieved in several ways. We opted to apply JointICA as it provides an elegant way to extract sources that link peaks separated in the EEG to regions in the fMRI based on across-subject variability. As the original method would decompose an EEG-fMRI dataset for each condition separately, we also modified the JointICA approach to estimate weighting matrices simultaneously for all stimulus conditions. With this modification, the method is able to pinpoint where and when different stimulus types elicited similar or distinct patterns of activity. In addition, the modified JointICA method allows for a quantitative comparison of individual components in a principled and unbiased way. Results from the modified JointICA confirm earlier findings but also provide novel insights in how perceptual grouping happens in the visual system, especially in combination with shape perception.

Let us start with a summary of the findings from the original JointICA (Figures 4-6). In the LG condition, the strong N1 from the ERP waveform is captured quite well with an IC reflecting widespread activation in the LOC around 200 ms after stimulus onset. This peak is seen to build up from 70 ms onwards with activity shifting forwards along the ventral stream. In the GO condition,

where the global shape is more difficult to see because it is not supported by simple pairwise contour linking between neighboring Gabor elements, ventral stream activity emerges later in time, with much weaker LOC activation throughout. Moreover, this condition induces a much later negative peak around 330 ms, involving a loop between LOC and EVA, which was completely absent in the LG condition. At this stage, an information exchange between EVA and LOC is probably taking place to establish a shape percept at a higher level (LOC), while trying to use as many of the oriented elements (signaled in EVA) as possible, which are compatible with a globally closed contour. In the NC condition, where no contour, neither locally nor globally defined, is present whatsoever, activations are still weaker and a small positive peak arises quite late after stimulus onset (around 370 ms), which appears to be accompanied by EVA activity again.

The results clearly show that the visual processing of a contour-defined shape is not merely a spatiotemporal shift of activity from early retinotopic to later occipitotemporal areas. Rather, it involves a dynamic interplay between these areas, in which the exact areas involved and the dynamics of their interplay depend on the specific stimulus condition. The modified JointICA allows to visualize this interplay in a more refined way. Focusing on the results shown in Figure 7, visual processing starts in V1-V2 around 70 ms, shifting forward to higher visual areas in the ventral stream around 170 ms. Around 240 ms, clear differences between the stimuli with structure (LG and GO) and the stimuli without structure (NC) appear. These results are consistent with earlier EEG studies (e.g., Machilsen et al., 2011; Mathes et al., 2006) and MEG studies (e.g., Tanskanen et al., 2008). This indicates that the first percept of some kind of structure that stands out from the background is accomplished around that time. However, that does not mean that processing stops at that point. At least in the condition where the shape is less well defined (the GO condition) because local edge linking is insufficient, an additional feedback loop occurs around 300 ms, which entails a reactivation of EVA. This could be interpreted as re-entrant processing where the visual system checks whether the local Gabor elements that form part of the groups established further in the cortical hierarchy

are really belonging to the same global shape represented in the LOC. The activations in V1 and V2 at such a later stage could indicate that (at least half of) the elements are not really locally "fitting" with the predictions generated at higher levels in the cortical hierarchy but only as a subset that fits a larger group in a hierarchical fashion, much as small Ls forming larger Hs in the Navon type of hierarchical stimuli (for reviews, see Kimchi, 1992; Navon, 2003). In the condition without a contour (NC) yet a later peak emerges, which also reflects EVA activity. This could reflect attentional enhancement as part of an attempt to verify whether there is really no structure there.

Consistent with previous findings in neurophysiology (Angelucci et al., 2002; McManus et al., 2011; Zhang & von der Heydt, 2010) and in human fMRI studies (Altmann et al., 2003; Kourtzi et al., 2003; Schwarzkopf et al., 2009), our results confirm the role of recurrent processing between high-level shape and object areas such as LOC and low-level retinotopic areas such as V1 and V2 in the integration of local elements into a global shape with a closed contour. A number of recent studies using fMRI have attempted to reveal how global shapes emerge from local elements along the cortical hierarchy, using fMRI adaptation (e.g., Kourtzi & Huberle, 2005) and fMRI multi-voxel pattern analysis or MVPA (e.g., Kubilius et al., 2011; Ostwald et al., 2008; Schwarzkopf et al., 2009). Although these studies differed widely with respect to the stimuli and tasks they employed, the overall conclusions were uniformly pointing towards sensitivity for local element attributes in the early visual areas and for global structure and shape properties in the higher occipitotemporal areas. However, the sluggish temporal resolution of fMRI did not allow to draw conclusions about the temporal dynamics of the information flow between these more locally interested areas and these more globally interested areas.

Mayhew et al. (2012) have recently used simultaneous EEG-fMRI measurements to unravel the spatiotemporal dynamics within the extended network involved in learning to discriminate different types of global structures in dot patterns with variable noise levels. Using MVPA on the activations in

the regions identified by EEG-informed fMRI mapping, these authors were able to distinguish learning in early processes involved in integration of local signals into more global forms in occipitotemporal and parietal areas from learning in later processes related to categorical decision making in frontal circuits. We used a different form of integrated fMRI-EEG data analysis, JointICA, for a different purpose. We wanted to understand the interplay between more local image analysis in the retinotopic visual areas and more global shape analysis in higher areas, and how this changes over time depending on the nature of the stimulus. We found that a more difficult type of structure emerges later in time and requires a more elaborate information exchange between lower and higher areas. We believe that such an iterative process plays a key role in extracting structure and constructing shape representations from natural images too, where clutter, noise, and occlusion all add to the complexity of contour integration.

In general, our findings fit quite well with more recent alternative views on the nature of the cortical hierarchy. Rather than assuming that there is always a fixed feedforward flow, which goes sequentially through all the stages along the ventral stream, low- and high-level areas do not necessarily engage exclusively in early and late aspects of processing, respectively. This view was made quite explicit in Hochstein and Ahissar's (2002) Reverse Hierarchy Theory, which involves a fast feedforward sweep, generating global percepts and high-level interpretation of the gist of the scene, followed by slower recurrent processing, integrating the local details within these top-down generated percepts when the task requires the fine resolution available at lower areas. Hence, early processing can occur at high levels in the visual system and low-level areas can be active during late processing (see also Lee et al., 1998; Roelfsema, 2006). A second larger theoretical framework that is consistent with our results is predictive coding (e.g., Friston, 2010; Rao & Ballard, 1999), which has already inspired a lot of interesting empirical work, both with fMRI (e.g., Alink et al., 2010; Fang et al., 2008; but see de-Wit et al., 2010, 2012 for discussion) and with neurophysiologically detailed models (Spratling, 2010). In short, the idea is that visual cortex is continuously updating its predictions about

the world, which are generated at higher levels, with only the mismatches or prediction errors being transmitted from low- to high-level areas. In terms of our study, this view would imply more activity in low-level areas in the more difficult condition with shapes defined only globally, with locally neighboring elements not being aligned and not fitting the global shape at the lower level in the hierarchy, which is exactly what we found. However, because this interpretation is largely speculative at this point, it awaits further confirmation from additional experiments specifically designed to test it.

Acknowledgements

We thank Jessica Bulthé and Christophe Bossens for assisting in the data collection, Ron Peeters for technical support during scanning, and Annelies Baeck, Vanja Van Aarsen and Peter Stiers for their help in the ROI definitions. We also thank the editor and the reviewers for comments that helped to improve the paper. This research is supported by the Research Council KUL: IDO/05/010 (EEG-fMRI integration), GOA MaNet and PFV/10/002 (OPTEC)*;* IUAP P719 (DYSCO, 2012–2017); the Flemish Government: FWO project G.0427.10N Integrated EEG-fMRI, IWT-TBM080658-MRI (EEG-fMRI) and iMinds. B. Mijović is supported by a PDM postdoctoral fellow of KU Leuven, Belgium. B. Machilsen is a postdoctoral fellow of the Research Foundation-Flanders. M. De Vos is supported by an Alexander von Humboldt grant and J. Wagemans by long-term structural funding from the Flemish Government (METH/08/02).

References

Alink, A., Schwiedrzik, C. M., Kohler, A., Singer, W., & Muckli, L. (2010). Stimulus predictability reduces responses in primary visual cortex. *The Journal of Neuroscience, 30,* 2960-2966.

Allen, P., Josephs, O., & Turner, R. (2000). A method for removing imaging artifact from continuous EEG recorded during functional MRI. *NeuroImage, 12*, 230–239.

Altmann, C.F., Bülthoff, H.H., & Kourtzi, Z. (2003). Perceptual organization of local elements into global shapes in the human visual cortex. *Current Biology, 13*(4), 342-349.

Angelucci, A., & Bressloff, P.C. (2006). Contribution of feedforward, lateral and feedback connections to the classical receptive field center and extra-classical receptive field surround of primate V1 neurons. *Progress in Brain Research, 154,* 93-120.

Angelucci, A., Levitt, J.B., Walton, E.J., Hupé, J.M., Bullier, J., & Lund, J.S. (2002). Circuits for local and global signal integration in primary visual cortex. *The Journal of Neuroscience, 22,* 8633-8646.

Calhoun, V.D., Adali, T., Pearlson, G.D., & Kiehl, K.A. (2006). Neuronal chronometry of target detection: Fusion of hemodynamic and event-related potential data. *NeuroImage, 30,* 544-553.

Debener, S., Ullsperger, M., Siegel, M., & Engel, A. (2006). Single-trial EEG-fMRI reveals the dynamics of cognitive function. *Trends in Cognitive Sciences, 10*(12), 558–563. doi:10.1016/j.tics.2006.09.010

Delorme, A., & Makeig, S. (2004). EEGLAB: an open source toolbox for analysis of single-trial EEG dynamics including independent component analysis. *Journal of Neuroscience Methods, 134*, 9–21.

Demeyer, M., & Machilsen, B. (2012). The construction of perceptual grouping displays using GERT. *Behavior Research Methods, 44*(2)*,* 439-446.

De Vos, M., De Lathauwer, L., & Van Huffel, S. (2011). Spatially constrained ICA algorithms with applications in EEG processing. *Signal Processing*, *91*(8), 1963-1972.

de-Wit, L. H., Machilsen, B., & Putzeys, T. (2010). Predictive coding and the neural response to predictable stimuli. *The Journal of Neuroscience, 30,* 8702-8703.

de-Wit, L. H., Kubilius, J., Wagemans, J., & Op de Beeck, H. P. (2012). Bi-stable Gestalts reduce activity in the whole of V1 not just the retinotopically predicted parts. *Journal of Vision, 12*(11):12, 1-14, doi: 10.1167/12.11.12.

Elder, J. H., & Goldberg, R. M. (2002). Ecological statistics of Gestalt laws for the perceptual organization of contours. *Journal of Vision, 2*(4):5, 324-353.

Fang, F., Kersten, D., & Murray, S. O. (2008). Perceptual grouping and inverse fMRI activity patterns in human visual cortex. *Journal of Vision, 8*(7):2, 1–9, doi:10.1167/8.7.2.

Field, D.J., Hayes, A., & Hess, R.F. (1993). Contour integration by the human visual system: Evidence for a local "association field". *Vision Research, 33,* 173-193.

Fitzpatrick, D. (1996). The functional organization of local circuits in visual cortex: Insights from the study of tree shrew striate cortex. *Cerebral Cortex, 6,* 329-341.

Friston, K. (2010). The free-energy principle: a unified brain theory? *Nature Reviews Neuroscience*, *11*(2), 127-138.

Gläscher, J. (2009). Visualization of Group Inference Data in Functional Neuroimaging. *Neuroinformatics, 7,* 73-82.

Geisler, W.S. (2008). Visual perception and the statistical properties of natural scenes. *Annual Review of Psychology, 59,* 167-192.

Grill-Spector, K., Kushnir, T., Hendler, T., Edelman, S., Itzchak, Y., & Malach, R. (1998). A sequence of object-processing stages revealed by fMRI in the human occipital lobe. *Human Brain Mapping, 6,* 316-328.

Hess, R.F., & Field, D.J. (1999). Integration of contours: New insights. *Trends in Cognitive Sciences, 3,* 480-486.

Hess, R.F., Beaudot, W.H., & Mullen, K.T. (2001). Dynamics of contour integration. *Vision Research, 41,* 1023-1037.

Himberg, J., Hyvärinen, A., & Esposito, F. (2004). Validating the independent components of neuroimaging time-series via clustering and visualization. *NeuroImage, 22,* 1214-1222.

Hochstein, S., & Ahissar, M. (2002). View from the top: hierarchies and reverse hierarchies in the visual system. *Neuron, 36,* 791-804. http://dx.doi.org/10.1016/S0896-6273(02)01091-7

Huster, R.J., Debener, S., Eichele, T., Herrmann, C.S. (2012). Methods for simultaneous EEG-fMRI : An introductory review. *The Journal of Neuroscience*, 32(18), 6053-6060.

Joyce, C., Gorodnitsky, I., & Kutas, M. (2004). Automatic removal of eye movement and blink artifacts from EEG data using blind component separation. *Psychophysiology, 41*(2), 313–325.

Kao, M., Mandal, A., Lazar, N., & Stufken, J. (2009). Multi-objective optimal experimental designs for event-related fMRI studies. *NeuroImage, 44,* 849-856.

Kimchi, R. (1992). Primacy of wholistic processing and global/local paradigm: A critical review. *Psychological Bulletin, 112,* 24-38.

Koffka, K. (1935). *Principles of Gestalt psychology*. London: Routledge & Kegan Paul.

Kourtzi, Z., Tolias, A.S., Altmann, C.F., Augath, M., & Logothetis, N.K. (2003). Integration of local features into global shapes: Monkey and human fMRI studies. *Neuron, 37*(2), 333-346.

Kourtzi, Z., & Huberle, E (2005). Spatiotemporal characteristics of form analysis in the human visual cortex revealed by rapid event-related fMRI adaptation. *NeuroImage*, 28, 440-452.

Kovács, I., & Julesz, B. (1993). A closed curve is much more than an incomplete one: Effect of closure in figure-ground segmentation. *Proceedings of the National Academy of Sciences of the United States of America, 90,* 7495-7497.

Kubilius, J., Wagemans, J., & Op de Beeck, H. P. (2011). Emergence of perceptual Gestalts in the human visual cortex: The case of the configural superiority effect. *Psychological Science, 22,* 1296-1303. http://dx.doi.org/10.1177/0956797611417000

Lee, T. S., Mumford, D., Romero, R., & Lamme, V. A. F. (1998). The role of the primary visual cortex in higher level vision. *Vision Research, 38,* 2429-2454. http://dx.doi.org/10.1016/S0042-6989(97)00464-1

Li, W., & Gilbert, C.D. (2002). Global contour saliency and local colinear interactions. *Journal of Neurophysiology, 88,* 2846-2856.

Li, W., Piëch, V., & Gilbert, C.D. (2008). Learning to link visual contours. *Neuron, 57*(3), 442-451.

Machilsen, B., Noviskiy, N., Vancleef, K., & Wagemans, J. (2011). Context modulates the ERP signature of contour integration. *PLoS ONE, 6(9)*, e25151.

Mathes, B., Trenner, D., & Fahle, M. (2006). The electrophysiological correlate of contour integration is modulated by task demands. *Brain Research, 1114*(1), 98-112.

Mayhew, S. D., Li, S., & Kourtzi, Z. (2012). Learning acts on distinct processes for visual form perception in the human brain. *The Journal of Neuroscience,* 32(3), 775-786.

McManus, J.N.J., Li, W., & Gilbert, C.D. (2011). Adaptive shape processing in primary visual cortex. *Proceedings of the National Academy of Sciences USA, 108,* 9739-9746.

Mijović, B., Vanderperren, K., Novitskiy, N., Vanrumste, B., Stiers, P., Van den Bergh, B., Wagemans, J., Lagae, L., Sunaert, S., Van Huffel, S., & De Vos, M. (2012). The "why" and "how" of JointICA: Results from a visual detection task. *NeuroImage, 60*, 1171-1185.

Moosmann, M., Schonfelder, V., Specht, K., Scheeringa, R., Nordby, H., & Hugdahl, K. (2009). Realignment parameter-informed artefact correction for simultaneous EEG-fMRI recordings. *NeuroImage, 45*, 1144–1150.

Navon, D. (2003). What does a compound letter tell the psychologist's mind? *Acta Psychologica, 114,* 273-309.

Niazy, R., Beckmann, C., Iannetti, G., Brady, J., & Smith, S. (2005). Removal of fMRI environment artifacts from EEG data using optimal basis sets. *NeuroImage, 28*, 720–737.

Ostwald, D., Lam, J. M., Li, S., & Kourtzi, Z. (2008). Neural coding of global form in the human visual cortex. *Journal of Neurophysiology*, 99, 2456-2469.

Pettet, M.W., McKee, S.P., & Grzywacz, N.M. (1998). Constraints on long range interactions mediating contour detection. *Vision Research, 38,* 865-879.

Pettet, M.W. (1999). Shape and contour detection. *Vision Research, 39,* 551-557.

Polat, U., Mizobe, K., Pettet, M.W., Kasamatsu, T., & Norcia, A.M. (1998). Collinear stimuli regulate visual responses depending on cell's contrast threshold. *Nature, 391,* 580-584.

Rao, R. P. N., & Ballard, D. H. (1999). Predictive coding in the visual cortex: A functional interpretation of some extra-classical receptive-field effects. *Nature Neuroscience, 2*(1), 79–87, doi:10.1038/4580

Roelfsema, P. R. (2006). Cortical algorithms for perceptual grouping. *Annual Review of Neuroscience, 29,* 203-277. http://dx.doi.org/10.1146/annurev.neuro.29.051605.112939

Rotermund, D., Schipper, M., Fahle, M., & Ernst, U.A. (2011). High-performance classification of contour percepts from EEG recordings. *BMC Neuroscience, 12(Suppl 1)*:P94.]

Schmidt, K.E., Goebel, R., Löwel, S., & Singer, W. (1997). The perceptual grouping criterion of colinearity is reflected by anisotropies of connections in the primary visual cortex. *European Journal of Neuroscience, 9,* 1083-1089.

Spratling, M. W. (2010). Predictive coding as a model of response properties in cortical area V1. *The Journal of Neuroscience, 30,* 3531-3543.

Schwarzkopf, D.S., Zhang, J. & Kourtzi, Z. (2009). Flexible learning of natural statistics in the human brain. *Journal of Neurophysiol*, 102, 1854-1867.

Tanskanen, T., Saarinen, J., Parkkonen, L., & Hari, R. (2008). From local to global: Cortical dynamics of contour integration. *Journal of Vision, 8*(7:15), 1-12.

Vanderperren, K., De Vos, M., Ramautar, J.R., Novitskiy, N., Mennes, M., Assecondi, S., Vanrumste, B., Van den Bergh, B.R., Wagemans, J., Lagae, L., Sunaert, S., & Van Huffel, S. (2010). Removal of BCG artifacts from EEG recordings inside the MR scanner: A comparison of methodological and validation-related aspects. *NeuroImage, 50*, 920–934.

Wagemans, J., Elder, J.H., Kubovy, M., Palmer, S.E., Peterson, M.A., Singh, M., & von der Heydt, R. (2012). A century of Gestalt psychology in visual perception: I. Perceptual grouping and figure-ground organization. *Psychological Bulletin, 138,* 1172-1217.

Wertheimer, M. (1923). Untersuchungen zur Lehre von der Gestalt. *Psychologische Forschung, 4,* 301-350.

Zhang, N. R., & von der Heydt, R. (2010). Analysis of the context integration mechanisms underlying figure-ground organization in the visual cortex. *The Journal of Neuroscience, 30,* 6482-6496. http://dx.doi.org/10.1523/JNEUROSCI.5168-09.2010

8. Table 1

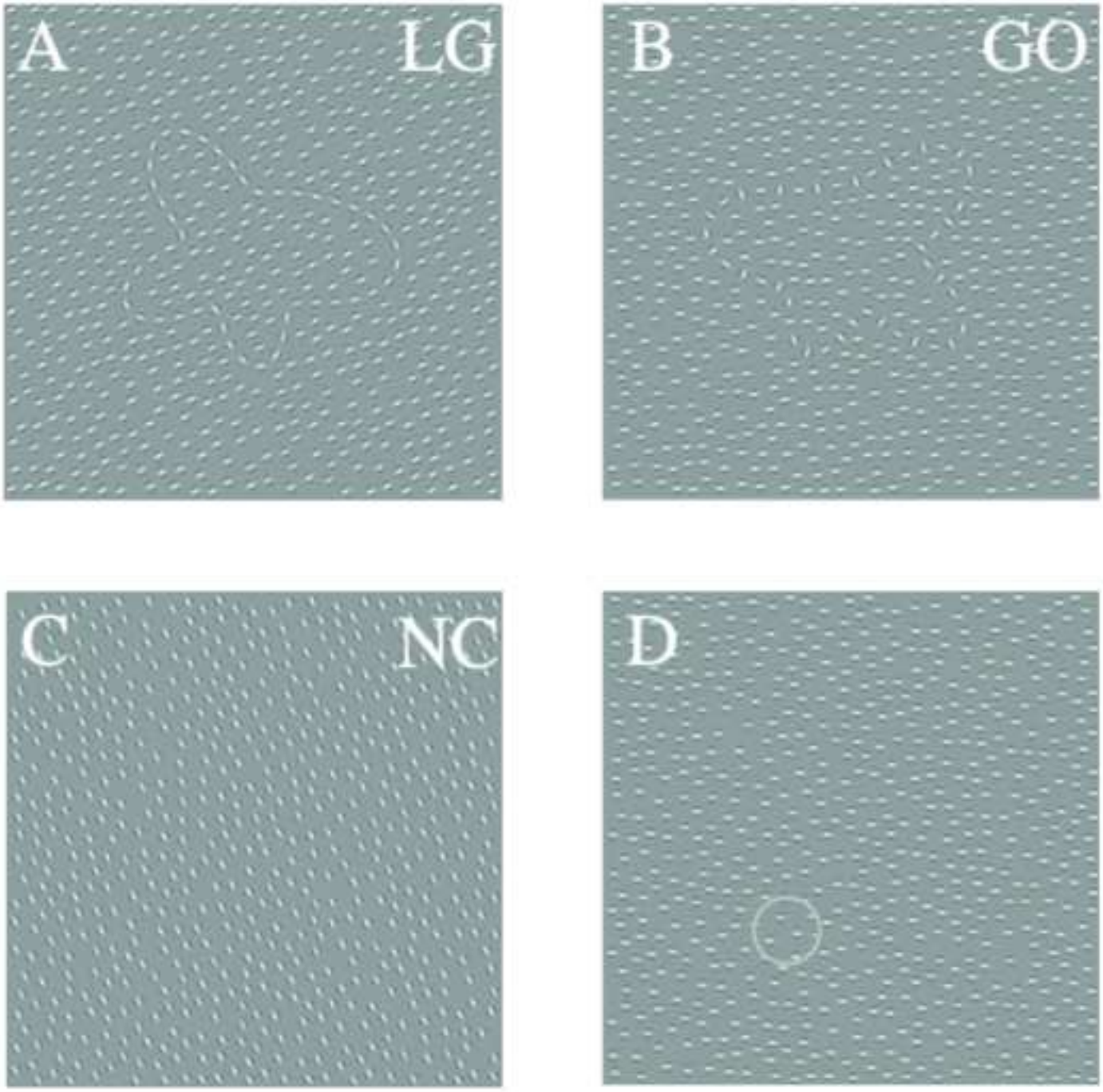
	Area	MNI	T-Scores
LG	EVA	11 -94 -3	14
	LOC	39 -87 -1	11.8
GO	EVA	9 -94 5	13.2
	LOC	35 -85 4	12
NC	EVA	12 -94 -3	8.4
	LOC	30 -92 5	9.9

8. Table 2

Component	Condition	Strength	MNI Coordinates	ROI
70ms	LG	4.4	15,-93,12	EVA
		3.35	36,-90,-7	LOC
	GO	4.39	13,-96,-2	EVA
			-	LOC
	NC	4.16	12,-91,-10	EVA
			-	LOC
170ms	LG	4.67	14,-91,-11	EVA
		3.9	44,-83,-7	LOC
	GO	4.87	14,-91,-11	EVA
		4.73	41,85,-6	LOC
	NC	5.74	14,-92,-11	EVA
		3.8	41,-75,-13	LOC
200ms	LG		-	EVA
		5.74	34,-90,-3	LOC
	GO		-	EVA
		5.56	35,-90,-6	LOC
	NC		-	EVA
		5.84	34,-90,-6	LOC
240ms	LG	3.7	11,-90,-11	EVA
		3.91	39,-85,-10	LOC
	GO	3.23	11,-94,-5	EVA
		3.17	37,-82,-14	LOC
	NC		-	EVA
			-	LOC
330ms	LG		-	EVA
			-	LOC
	GO	4,61	11,-92,15	EVA
		5.43	40,-86,-6	LOC
	NC		-	EVA
			-	LOC
370ms	LG	3.71	12,95,-2	EVA
		3.71	39,-71,-14	LOC
	GO	5.21	7,-76,12	EVA
		4.82	39,-71,-14	LOC
	NC	5.89	10,-91,-6	EVA
			-	LOC

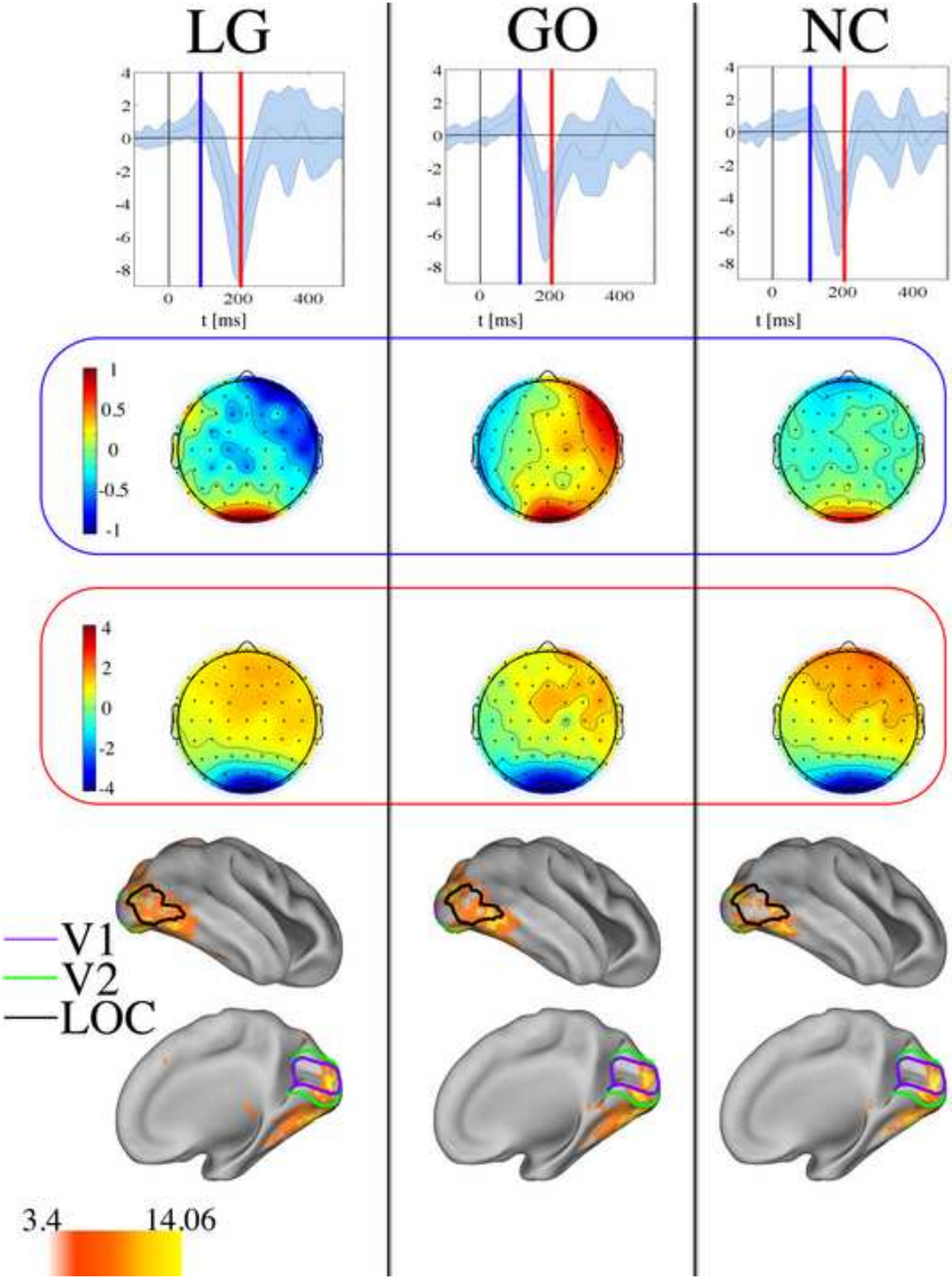
9. Figure 1

Click here to download high resolution image



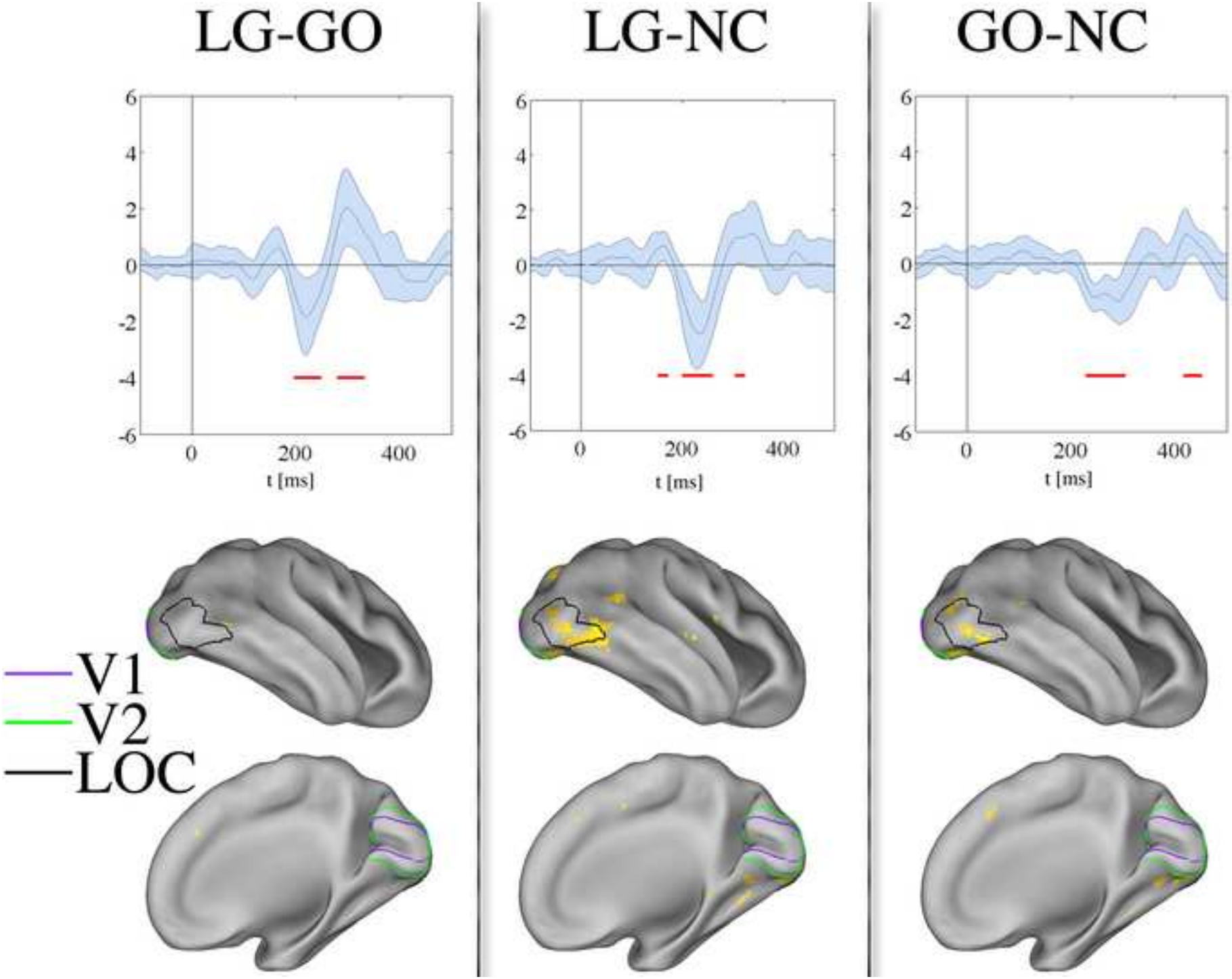
9. Figure 2

Click here to download high resolution image



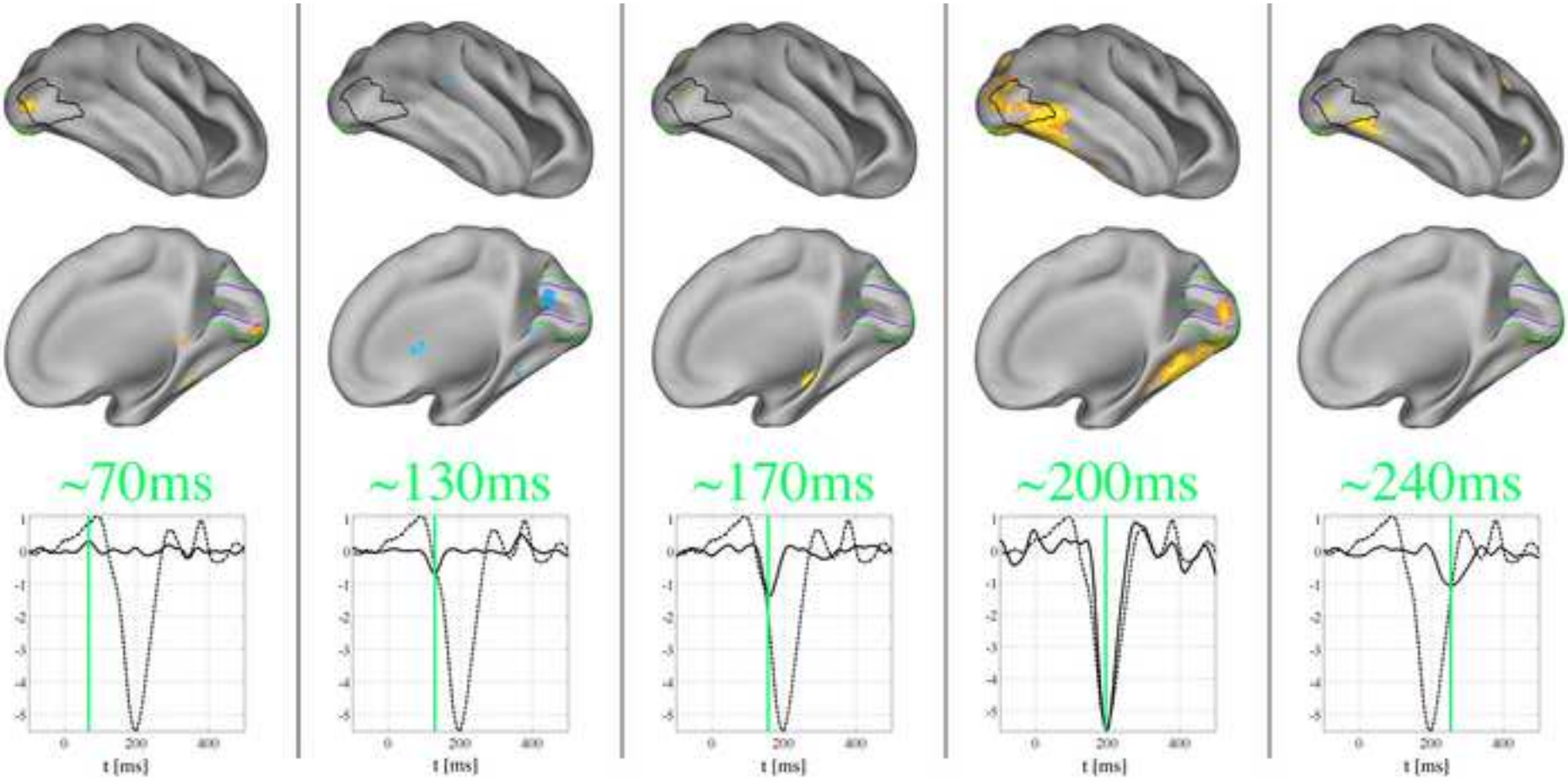
9. Figure 3

Click here to download high resolution image



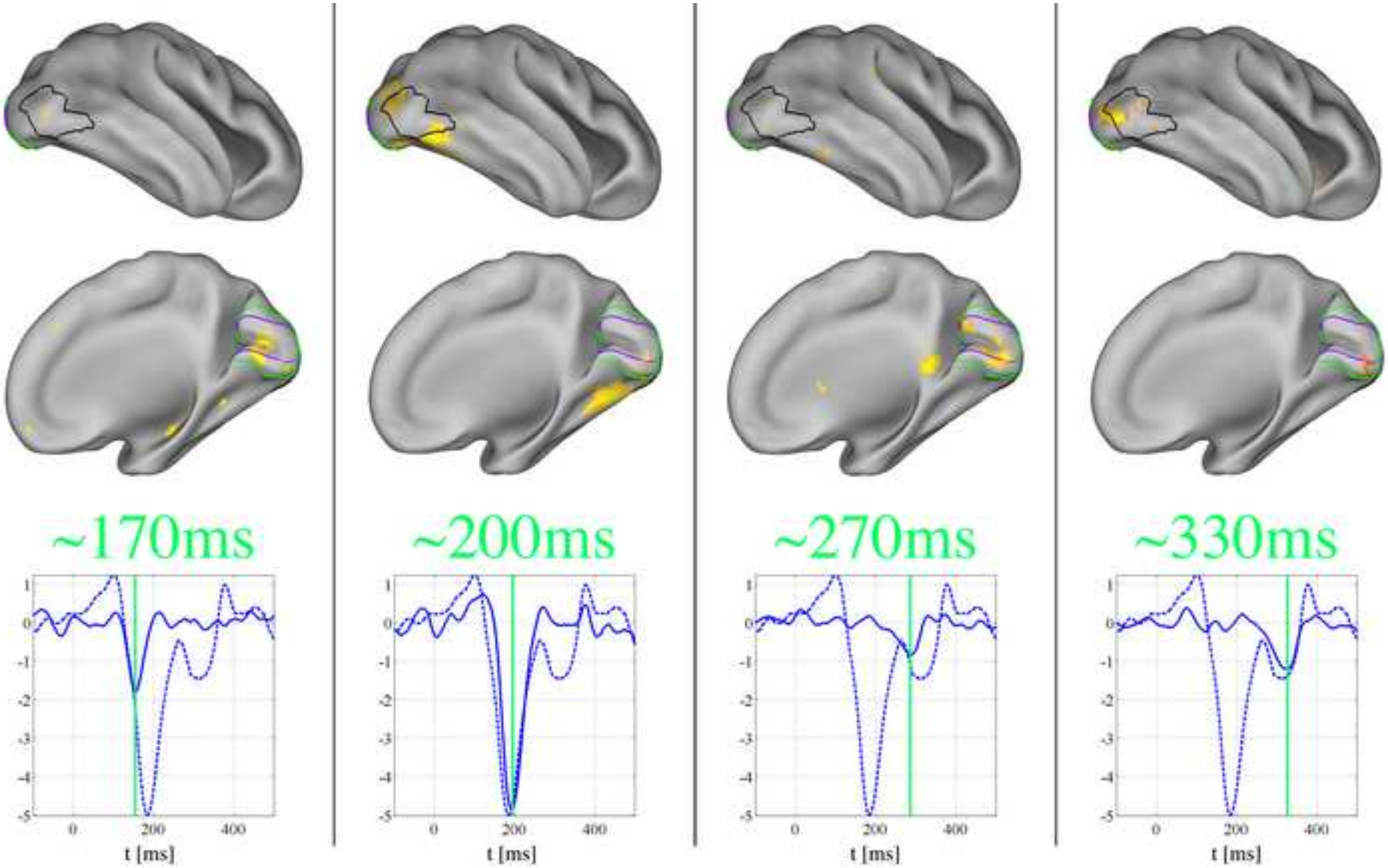
9. Figure 4

Click here to download high resolution image



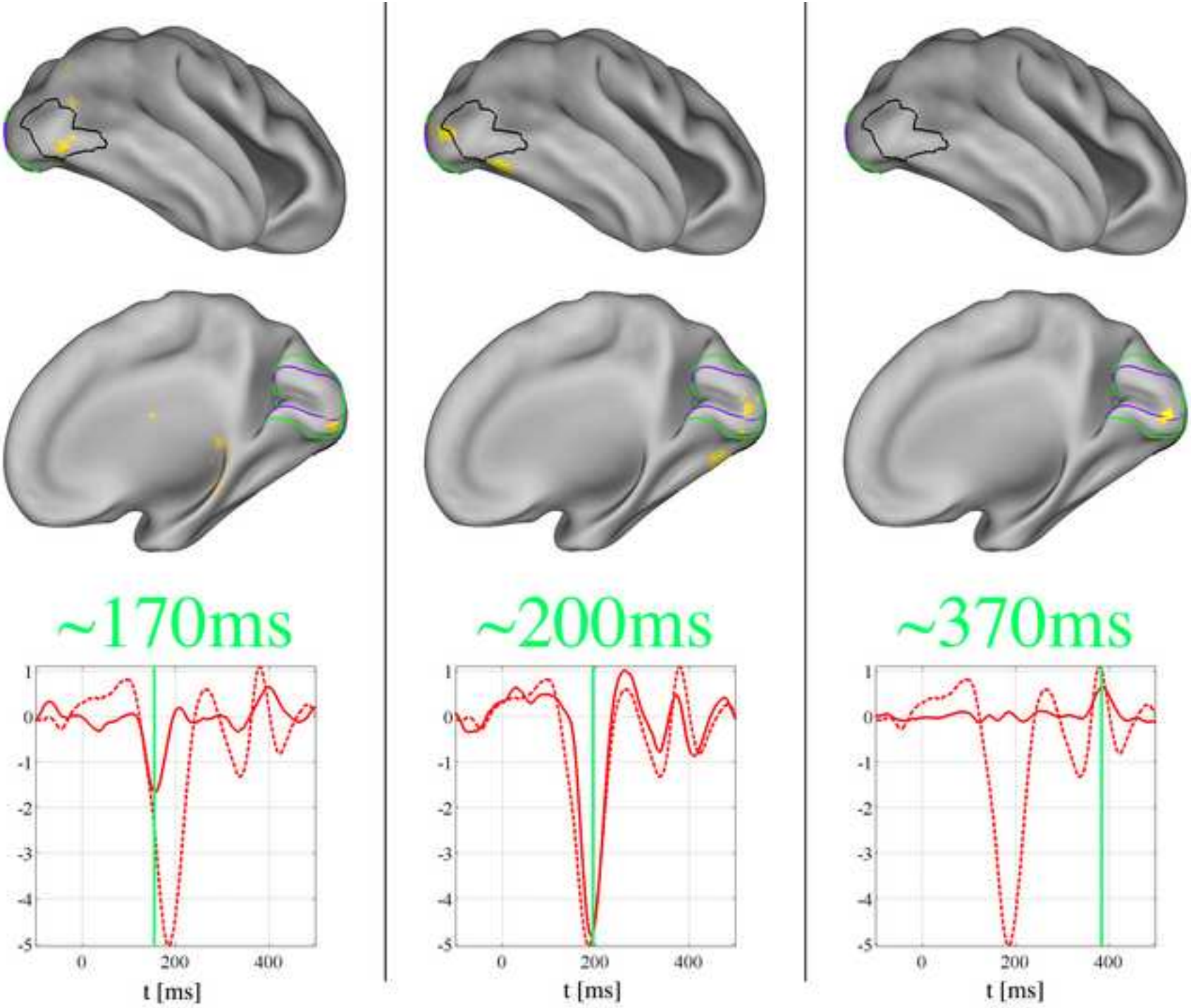
9. Figure 5

Click here to download high resolution image



9. Figure 6

Click here to download high resolution image



9. Figure 7

Click here to download high resolution image

